An MIQP model for microgrid unit commitment incorporating grid-connected/islanded operating modes and power network

Nguyen Thi Hoai Thu[1], Pham Nang Van[1*]

[1] *School of Electrical and Electronic Engineering, Hanoi University of Science and Technology, Hanoi, Vietnam*
[*] *Corresponding author E-mail: van.phamnang@hust.edu.vn*

Abstract

This paper presents a mixed-integer quadratic programming (MIQP) model to address the day-ahead unit commitment (UC) problem for microgrids. The microgrid in this study includes conventional generators (CGs), renewable energy sources, and energy storage systems. The transition between grid-connected and islanded operating modes, as well as power grid constraints, is integrated into the proposed MIQP optimization model. The objective of the suggested formulation is to minimize the total operating costs of the microgrid, including the operating costs of conventional generating units and the expenses of purchasing electricity from the main grid. The MIQP model is derived from a mixed-integer nonlinear programming (MINLP) model by linearizing the product of two continuous variables and quadratic elements. The proposed MIQP model is implemented using the GAMS language with the commercial solver CPLEX and evaluated on a modified IEEE 33-node microgrid. The computational results demonstrate the effectiveness of the proposed optimization approach.

Keywords*: Unit commitment (UC), Microgrid (MG), Mixed-Integer Quadratic Programming (MIQP), Renewable Energy; Energy storage devices (ESD)*

Abbreviations

MIQP	Mixed-Integer Quadratic Programming
CG	Conventional Generators
MINLP	Mixed-Integer Nonlinear Programming
UC	Unit Commitment
DG	Distributed Generation
MILP	Mixed-Integer Linear Programming
ESD	Energy Storage Devices
MC	Microgrid

1. Introduction

With continuous advancements in science and technology, the increasing demand for electricity has become a significant challenge. A promising solution to address this challenge is the integration of distributed generation (DG) sources into the existing power grid, which has facilitated the development of microgrids (MGs). A microgrid is a small-scale power network comprising electrical loads, conventional power sources, renewable energy sources (RES), and energy storage systems. Importantly, microgrids can operate in either grid-connected or islanded modes, depending on technical and economic considerations [1]. Microgrids offer several advantages, including operational flexibility, the ability to operate independently, and reduced operational costs compared to traditional power grids. Therefore, precise and efficient planning of power source operations is critical to maximizing the economic benefits of microgrids. The unit commitment (UC) problem plays a critical role in power system operations, as it ensures a stable and uninterrupted electricity supply while meeting economic objectives for loads in microgrids. As a result, numerous optimization models addressing the UC problem in microgrids have been extensively studied.

In their research, Van et al. [2] proposed a Mixed-Integer Linear Programming (MILP) model based on a Mixed-Integer Nonlinear Programming (MINLP) model by applying linearization techniques for power loss. The objective of their study was to determine the operating states of generation units to maximize total social benefits over a fixed time period. Similarly, another study [3] introduced a power flow analysis method for microgrids in islanded operation mode, incorporating the cost characteristics of power sources. In paper [4], Li et al. employed heuristic optimization algorithms such as MOMFO to minimize the operational costs of power sources. Furthermore, the paper [5] presented methods for determining the optimal locations of distributed generation sources to minimize both investment and operational costs in microgrids.

In research [6], the authors proposed an MILP model for energy management systems (EMS) of microgrids operating in both grid-connected and islanded modes. The MILP model in study [5] was developed based on the MINLP model using piecewise linearization techniques. Paper [7] utilized a Mixed-Integer Quadratic Programming (MIQP) model for frequency regulation combined with the unit commitment planning of standalone microgrids, significantly reducing the operational costs of distributed energy sources. Study [8] proposed differential evolution (DE) and particle swarm optimization (PSO) techniques to determine the optimal placement and quantity of distributed energy sources in microgrids. The study [9] established a model of optimization for operation trading strategies that consider multiple levels of energy-certificate-carbon market linkage in multi-microgrid networks. The suggested technique establishes a combined MMG two-tier certificate-carbon trading system grounded in the uniqueness principle, thus circumventing the double-counting issue

Received: 04-01-2025; Accepted: 15-03-2025.

associated with renewable energy advantages. Paper [10] introduced a novel supervised learning technique for the real-time optimum electrical energy scheduling of an autonomous microgrid. The study [11] introduced an operation decision-making methodology with secure privacy for independent microgrids interconnected through an electrical distribution network, wherein the distribution network operator and microgrid master controllers independently make choices as distinct entities. The work [12] presented a bi-level framework based on quadratic programming with integer variables (MIQP) for the optimum management of microgrids under the most severe cases of renewable energy source interruptions. Authors in [13] put forward a bi-level distributed optimization strategy for the operation of linked microgrid systems under uncertainty, aimed at optimally coordinating the operations of microgrids owned by several stakeholders in a market context.

The objective of this study is to present a method for accurately and efficiently planning the operation of power sources to maximize the economic benefits of microgrids. In this research, the authors propose an optimal operation planning method that considers grid constraints and the grid-connected/islanded operation modes of microgrids using MIQP. The objective function is quadratic, while the constraints are linear. The key contributions of this paper are summarized as follows:

- Proposed a MINLP model for the UC problem in microgrids, accounting for the transition between grid-connected and islanded operation modes, as well as grid constraints.
- Applied linearization techniques to develop an MIQP model for the UC problem in microgrids.
- Examined the impact of grid-connected/islanded operation modes on optimal operation planning in microgrids.

The paper is structured into three main sections. Section 2 presents the research methodology, including the development of the MIQP model for day-ahead operation scheduling considering grid constraints in microgrids, and the linearization techniques for nonlinear constraints. Section 3 provides computational results and discussions when the model is applied to the 33-bus IEEE microgrid system. Finally, conclusions and future research directions are presented in Section 4.

2. Methodology

2.1. MINLP model for the UC problem

2.1.1. *Objective function*

The objective function for the day-ahead operation planning problem, which considers grid constraints in a microgrid, is to minimize the total operational costs of the power sources.

$$\min \sum_{t=1}^{T} \left\{ \begin{array}{l} \sum_{i=1}^{N_{CG}} \left[\begin{array}{l} c_i^{\mathrm{SU,CG}} y_{i,t} + c_i^{\mathrm{SD,CG}} x_{i,t} \\ +\alpha_i u_{i,t} + \beta_i P_{i,t}^{\mathrm{CG}} + \gamma_i \left(P_{i,t}^{\mathrm{CG}} \right)^2 \end{array} \right] \\ +c_i^{\mathrm{MG,B}} P_t^{\mathrm{sub,B}} - c_i^{\mathrm{MG,S}} P_t^{\mathrm{sub,S}} \end{array} \right\} \quad (1)$$

where:

- N_{CG} is the number of traditional power plants in the microgrid;
- $c_i^{\mathrm{SU,CG}}$ and $c_i^{\mathrm{SD,CG}}$ are the startup and shutdown costs of the *i*-th traditional power plant, respectively;
- $y_{i,t}$ is a binary variable. If the *i*-th traditional power plant starts up at the beginning of time *t*, then $y_{i,t} = 1$; otherwise, $y_{i,t} = 0$;
- $x_{i,t}$ is a binary variable. If the *i*-th traditional power plant shuts down at the beginning of time *t*, then $x_{i,t} = 1$; otherwise, $x_{i,t} = 0$;
- $u_{i,t}$ is a binary variable. If the *i*-th traditional power plant operates at the time *t*, then $u_{i,t} = 1$; otherwise, $u_{i,t} = 0$;
- α_i, β_i, and γ_i are the coefficients in the operating cost function of the *i*-th traditional power plant;
- $P_{i,t}^{\mathrm{CG}}$ is the output power of the *i*-th traditional power plant at time *t* (pu);
- $c_t^{\mathrm{MG,B}}$ and $c_t^{\mathrm{MG,S}}$ are the buying and selling prices of electricity between the microgrid and the distribution grid at time *t* ($/kWh).;
- $P_t^{\mathrm{sub,B}}$ và $P_t^{\mathrm{sub,S}}$ are the buying and selling power of the microgrid with the external grid at time *t* (pu);
- *T* is the total number of time intervals of the operational scheduling horizon.

2.1.2. *Power Exchange Constraints of the Microgrid with the Main Grid*

The power exchange constraints of the microgrid with the main grid are described in equations (2)–(5).

$$m_t z_t P_{\min}^{\mathrm{sub,B}} \le P_t^{\mathrm{sub,B}} \le m_t z_t P_{\max}^{\mathrm{sub,B}};\ t = 1,...,T \quad (2)$$

$$\left(1 - m_t\right) z_t P_{\min}^{\mathrm{sub,S}} \le P_t^{\mathrm{sub,S}} \le \left(1 - m_t\right) z_t P_{\max}^{\mathrm{sub,S}};\ t = 1,...,T \quad (3)$$

$$m_t \in \{0,1\};\ t = 1,...,T \quad (4)$$

$$\frac{P_t^{\mathrm{sub,B}} + P_t^{\mathrm{sub,S}}}{\sqrt{\left(P_t^{\mathrm{sub}}\right)^2 + \left(Q_t^{\mathrm{sub}}\right)^2}} \ge \cos\varphi_{\min}^{\mathrm{sub}}\ t = 1,...,T \quad (5)$$

where:

- $P_{\max}^{\mathrm{sub,B}}$ and $P_{\max}^{\mathrm{sub,S}}$ are the maximum power purchase and sale limits of the microgrid (pu);
- $P_{\min}^{\mathrm{sub,B}}$ and $P_{\min}^{\mathrm{sub,S}}$ are the minimum power purchase and sale limits of the microgrid (pu);
- m_t is a binary variable. If the MG purchases electricity from the main grid at time *t*, then $m_t = 1$. Similarly, if the microgrid sells electricity to the main grid at time *t*, then $m_t = 0$;
- $z_t = 1.$ is a predefined binary constant. If the MG operates in grid-connected mode at time *t*, then $z_t = 1$. If it operates in islanded mode at time *t*, then $z_t = 0$.
- $\cos\varphi_{\min}^{sub}$ is the required power factor at the point of connection;

- P_t^{sub} and Q_t^{sub} are the active and reactive power flows between the substation node and the microgrid (pu), respectively.

Constraints (2) and (3) set the limits on the power purchase and sale of the microgrid with the main grid, respectively. Constraint (4) introduces a binary condition to ensure that electricity purchase and sale cannot occur simultaneously. Meanwhile, constraint (5) ensures that the power factor of the microgrid stays within the permissible range.

2.1.3. *Constraints of Traditional Power Sources*

Constraints of Traditional Power Sources can be illustrated through (6) – (16).

$$u_{i,t}P_{i,\min}^{\mathrm{CG}} \le P_{i,t}^{\mathrm{CG}} \le u_{i,t}P_{i,\max}^{\mathrm{CG}}\ ; \forall i \in \Omega_{\mathrm{CG}}; t = 1,...,T \quad (6)$$

$$\sum_{i\in\Omega_{\mathrm{CG}}} P_{i,\max}^{\mathrm{CG}}u_{i,t} + \sum_{i\in\Omega_{\mathrm{PV}}} P_{i,t}^{\mathrm{PV}} + \sum_{i\in\Omega_{\mathrm{W}}} P_{i,t}^{\mathrm{W}} + \sum_{i\in\Omega_{\mathrm{EDS}}} \left(P_{i,t}^{\mathrm{Ch}} - P_{i,t}^{\mathrm{Dch}}\right) \ge P_t^{\mathrm{R}} + \sum_{i\in\Omega_{\mathrm{D}}} P_{i,t}^{\mathrm{D}}\ ; t = 1,...,T \quad (7)$$

$$\frac{P_{i,t}^{\mathrm{CG}}}{\sqrt{\left(P_{i,t}^{\mathrm{CG}}\right)^2 + \left(Q_{i,t}^{\mathrm{CG}}\right)^2}} \ge \cos\varphi_{i,\min}^{\mathrm{CG}};\ \forall i \in \Omega_{\mathrm{CG}}; t = 1,...,T \quad (8)$$

$$P_{i,t}^{\mathrm{CG}} - P_{i,t-1}^{\mathrm{CG}} \le R_i^{\mathrm{SU,CG}}y_{i,t} + R_i^{\mathrm{U,CG}}u_{i,t-1};\ \forall i \in \Omega_{\mathrm{CG}}; t = 1,...,T \quad (9)$$

$$P_{i,t-1}^{\mathrm{CG}} - P_{i,t}^{\mathrm{CG}} \le R_i^{\mathrm{SD,CG}}x_{i,t} + R_i^{\mathrm{D,CG}}u_{i,t};\ \forall i \in \Omega_{\mathrm{CG}}; t = 1,...,T \quad (10)$$

$$u_{i,t} - u_{i,t-1} = y_{i,t} - x_{i,t}\ ;\ \forall i \in \Omega_{\mathrm{CG}}; t = 1,...,T \quad (11)$$

$$x_{i,t}, y_{i,t}, u_{i,t} \in \{0,1\}\ ; \forall i \in \Omega_{\mathrm{CG}}; t = 1,...,T \quad (12)$$

$$y_{i,t} + x_{i,t} \le 1\ ; \forall i \in \Omega_{\mathrm{CG}}; t = 1,...,T \quad (13)$$

$$u_{i,0} = U_{i,0}^{CG}\ ;\ \forall i \in \Omega_{\mathrm{CG}} \quad (14)$$

$$\sum_{k=t-T_i^{\mathrm{U}}+1,k\ge 1}^{t} y_{i,k} \le u_{i,t}\ ; \forall t \in \left[L_t - 1,...,T\right]; \forall i \in \Omega_{\mathrm{CG}} \quad (15)$$

$$u_{i,t} + \sum_{k=t-T_i^{D}+1,k\ge 1}^{t} x_{i,k} \le 1\ ; \forall t \in \left[F_t - 1,...,T\right]; \forall i \in \Omega_{\mathrm{CG}} \quad (16)$$

where:

- Ω_{CG} is the set of nodes connected to traditional power sources.;
- Ω_{D} is the set of nodes connected to loads;
- $P_{i,\min}^{\mathrm{CG}}$ and $P_{i,\max}^{\mathrm{CG}}$ are the minimum and maximum active power outputs of the *i*-th power plant (pu), respectively.;
- $P_{i,t}^{\mathrm{R}}$ is the system's reserve power requirement at time *t* (pu), set as 20% of the total system load;
- $\cos\varphi_{i,\min}^{CG}$ is the power factor requirement at the connection point of the *i*-th traditional power source;
- $R_i^{\mathrm{D,CG}}$ and $R_i^{\mathrm{U,CG}}$ are the downward and upward ramping limits of the *i*-th power plant (pu), respectively;
- $R_i^{\mathrm{SU,CG}}$ and $R_i^{\mathrm{SD,CG}}$ are the startup ramping limit and shutdown ramping limit of the *i*-th power plant (pu), respectively;
- $U_{i,0}^{\mathrm{CG}}$ is the initial state of the traditional unit at node *i*;
- T_i^U and T_i^D are the minimum uptime and minimum downtime of the *i*-th power plant (hours), respectively.

The generation limits of traditional power sources are defined in constraint (6). The reserve power constraint is represented in expression (7). Expression (8) ensures compliance with the power factor at the connection point with the traditional power source. Expressions (9) and (10) limit power output changes to the ramping limits between consecutive time periods. Constraints (11)–(13) restrict operations such that active units can only shut down and non-operating units can only start up. Expression (14) defines the initial state of the *i*-th traditional power source. Constraints (15) and (16) enforce the minimum uptime and minimum downtime, where $L_i = \min\{T,U_i\}$ and $F_i = \min\{T,D_i\}$. Here, U_i is the number of time periods the *i*-th plant must operate at the start of the scheduling cycle, and D_i denotes the number of time periods the *i*-th plant must remain off at the start of the scheduling cycle.

2.1.4. *Constraints of Renewable Energy Sources*

The constraints of renewable energy sources are described in equations (17)–(20). Specifically, constraints (17) and (18) define the power generation limits of renewable energy sources, while constraints (19) and (20) ensure that the power factor of renewable energy sources remains within the allowable range.

$$0 \le P_{i,t}^{\mathrm{PV}} \le P_{i,t,\mathrm{forecast}}^{\mathrm{PV}}; \forall i \in \Omega_{\mathrm{PV}}; t = 1,...,T \quad (17)$$

$$0 \le P_{i,t}^{\mathrm{W}} \le P_{i,t,\mathrm{forecast}}^{\mathrm{W}}; \forall i \in \Omega_{\mathrm{W}}; t = 1,...,T \quad (18)$$

$$\frac{P_{i,t}^{\mathrm{PV}}}{\sqrt{\left(P_{i,t}^{\mathrm{PV}}\right)^2 + \left(Q_{i,t}^{\mathrm{PV}}\right)^2}} \ge \cos\varphi_{i,\min}^{\mathrm{PV}}; \forall i \in \Omega_{\mathrm{PV}}; t = 1,...,T \quad (19)$$

$$\frac{P_{i,t}^{\mathrm{W}}}{\sqrt{\left(P_{i,t}^{\mathrm{W}}\right)^2 + \left(Q_{i,t}^{\mathrm{W}}\right)^2}} \ge \cos\varphi_{i,\min}^{\mathrm{W}}; \forall i \in \Omega_{\mathrm{W}}; t = 1,...,T \quad (20)$$

where:

- Ω_{PV} và Ω_{W} are the sets of nodes connected to solar power (PV) and wind power (W) sources in the microgrid, respectively;
- $P_{i,t}^{\mathrm{PV}}$ and $P_{i,t}^{\mathrm{W}}$ are the active power outputs of solar power and wind power sources (pu), respectively;
- $P_{i,t,\mathrm{forecast}}^{\mathrm{PV}}$ and $P_{i,t,\mathrm{forecast}}^{\mathrm{W}}$ are the forecasted power outputs of solar power and wind power sources (pu), respectively;
- $\cos\varphi_{i,\min}^{\mathrm{PV}}$ and $\cos\varphi_{i,\min}^{\mathrm{W}}$ are the power factor requirements at the connection points of the *i*-th solar power and wind power sources, respectively.

2.1.5. *Constraints of Energy Storage Devices*

The energy storage device model presented in this paper is applicable to most energy storage systems using battery storage [14]. The constraints related to energy storage devices are described in equations (21)–(27):

$$E_{i,0} = E_{i,0}^{\mathrm{ESD}}\ ;\ \forall i \in \Omega_{\mathrm{ESD}} \quad (21)$$

$$E_{i,t} = E_{i,t-1} + \left(\eta_i^{\mathrm{Ch}} P_{i,t}^{\mathrm{Ch}} - \frac{1}{\eta_i^{\mathrm{Dch}}} P_{i,t}^{\mathrm{Dch}} \right).T_s; \quad \forall i \in \Omega_{\mathrm{ESD}}; t = 1,...,T \tag{22}$$

$$E_i^{\min} \le E_{i,t} \le E_i^{\max} \; ; \forall i \in \Omega_{\mathrm{ESD}}; t = 1,...,T \tag{23}$$

$$0 \le P_{i,t}^{\mathrm{Dch}} \le P_i^{\mathrm{Dch,max}} v_{i,t} \; ; \forall i \in \Omega_{\mathrm{ESD}}; t = 1,...,T \tag{24}$$

$$0 \le P_{i,t}^{\mathrm{Ch}} \le P_i^{\mathrm{Ch,max}} \left(1 - v_{i,t}\right) ; \forall i \in \Omega_{\mathrm{ESD}}; t = 1,...,T \tag{25}$$

$$v_{i,t} \in \{0,1\} \; ; \forall i \in \Omega_{\mathrm{ESD}}; t = 1,...,T \tag{26}$$

$$E_{i,t=T} = E_{i,t=0}; \; \forall i \in \Omega_{\mathrm{ESD}} \tag{27}$$

where:

- Ω_{ESD} : Set of nodes connected to energy storage devices.
- $E_{i,t}$: Energy level of storage device *i* at time *t* (pu).
- $E_{i,0}^{\mathrm{ESD}}$: Initial energy level of storage device *i* (pu).
- $E_i^{\max}$ and $E_i^{\min}$: Maximum and minimum storage energy levels (pu).
- $P_{i,t}^{\mathrm{Ch}}$ and $P_{i,t}^{\mathrm{Dch}}$: Charging and discharging power of storage device *i* at time *t* (pu).
- $P_{i,t}^{\mathrm{Ch,max}}$ and $P_{i,t}^{\mathrm{DCh,max}}$: Maximum charging and discharging power of storage device *i* (pu).
- η_i^{Ch} and η_i^{Dch} : Charging and discharging efficiencies of storage device *i*.
- T_s : Time step for the day-ahead scheduling problem (T_s =1 hour).
- $v_{i,t}$: Binary variable; $v_{i,t} = 1$ if the device is discharging at time *t*, $v_{i,t} = 0$ if the device is charging at time *t*.

Equation (21) specifies the initial energy state of the storage device, while Equation (22) determines the energy level at any given time *t*. Equation (23) defines the limits of energy levels, and Equations (24) and (25) constrain the discharge and charge power, respectively. Equation (26) ensures that charging and discharging cannot occur simultaneously, and Equation (27) maintains that the energy level at the start and end of the cycle is the same.

2.1.6. *Constraints of the Power Grid*

Constraints of the Power Grid are described in (28)–(33).

$$\sum_{k \in \Omega_{pr(i)}} \left(P_{ki,t} - r_{ki} I_{ki,t}^2 \right) - \sum_{j \in \Omega_{cr(i)}} P_{ij,t} = P_{i,t}^{\mathrm{D}} - P_{i,t}^{\mathrm{sub,B}} + P_{i,t}^{\mathrm{Ch}} + P_{i,t}^{\mathrm{sub,S}} - P_{i,t}^{\mathrm{Dch}} - P_{i,t}^{\mathrm{CG}} - P_{i,t}^{\mathrm{PV}} - P_{i,t}^{\mathrm{W}} \quad \forall i \in \Omega_{\mathrm{B}}; t = 1,...,T \tag{28}$$

$$\sum_{k \in \Omega_{pr(i)}} \left(Q_{ki,t} - x_{ki} I_{ki,t}^2 \right) - \sum_{j \in \Omega_{cr(i)}} Q_{ij,t} = Q_{i,t}^{\mathrm{D}} + Q_{i,t}^{\mathrm{sub,B}} - Q_{i,t}^{\mathrm{sub,S}} - Q_{i,t}^{\mathrm{CG}} - Q_{i,t}^{\mathrm{PV}} - Q_{i,t}^{\mathrm{W}}; \quad \forall i \in \Omega_{\mathrm{B}}; t = 1,...,T \tag{29}$$

$$U_{i,t}^2 - U_{j,t}^2 - 2\left(r_{ij} P_{ij,t} + x_{ij} Q_{ij,t} \right) + \left(r_{ij}^2 + x_{ij}^2 \right) I_{ij,t}^2 = 0 \quad \forall j \in \Omega_{cr(i)}; i \in \Omega_{\mathrm{B}}; t = 1,...,T \tag{30}$$

$$I_{ij,t}^2 U_{i,t}^2 = P_{ij,t}^2 + Q_{ij,t}^2; \; \forall i \in \Omega_{\mathrm{B}}; t = 1,...,T \tag{31}$$

$$0 \le I_{ij,t} \le I_{ij}^{\max} \; ; \forall j \in \Omega_{cr(i)}; i \in \Omega_{\mathrm{L}}; t = 1,...,T \tag{32}$$

$$U_{\min} \le U_{i,t} \le U_{\max} \; ; \forall i \in \Omega_{\mathrm{B}}; t = 1,...,T \tag{33}$$

where:

- $P_{i,t}^{\mathrm{D}}$ and $Q_{i,t}^{\mathrm{D}}$ are the active and reactive power demand, respectively, at node *i* at time *t* (pu);
- $P_{ij,t}$ and $Q_{ij,t}$ are the active and reactive power flow, respectively, on line *ij* at node *i* at time *t* (pu);
- $I_{ij,t}$ is the current on line branch *ij* (pu);
- $I_{ij}^{\max}$ is the maximum current limit on branch *ij* (pu);
- $U_{i,t}$ is the voltage at node *i* at time *t* (pu);
- $U_{\min}$ and $U_{\max}$ are the minimum and maximum voltage limits at nodes within the small grid (pu)
- r_{ij} and x_{ij} are the resistance and reactance, respectively, of line *ij* (pu);
- $\Omega_{pr(i)}$ is the set of nodes that directly connect to and supply power to node *i*;
- $\Omega_{cr(i)}$ is the set of nodes that directly connect to and receive power from node *i*;
- Ω_{L} is the set of all line nodes in the power grid;
- Ω_{L} is the set of all line branches in the power grid.

Equations (28) and (29) are the active and reactive power balance constraints between power sources, branch power flow, and loads at each node. Constraint (30) represents the relationship between the voltages of two directly connected nodes in the small power grid. Equation (31) describes the product of the square of the current on branch *ij* and the square of the voltage at node *i*, which equals the sum of the squares of active and reactive power on branch *ij*. Constraints (32) and (33) represent the current limit on line branches and the voltage limits at nodes, respectively.

As can be seen, the model has:

- The objective function (1) which is a nonlinear quadratic operating cost function;
- The power factor constraints at the point of connection (5), (8), (19), and (20) which are nonlinear;
- The power flow constraints for the grid (28) - (31), which are nonlinear.

Because the model is nonlinear and takes a long time to solve, this study will linearize the nonlinear constraints and build a MIQP model of the problem to shorten the solution time.

2.2. MIQP Model of the UC Problem Considering Grid Constraints

2.2.1. *Linearization of Power Limit Constraints at Connection Points*

As discussed in Section 2.1, the power factor constraints at the connection points (5), (8), (19), and (20) are nonlinear. Therefore, these constraints are linearized as follows:

$$-\frac{P_t^{\mathrm{sub}} \sqrt{1 - \left(\cos \varphi_{\min,\mathrm{lagging}}^{\mathrm{sub}}\right)^2}}{\cos \varphi_{\min,\mathrm{lagging}}^{\mathrm{sub}}} \le Q_t^{\mathrm{sub}} \le \frac{P_t^{\mathrm{sub}} \sqrt{1 - \left(\cos \varphi_{\min,\mathrm{leading}}^{\mathrm{sub}}\right)^2}}{\cos \varphi_{\min,\mathrm{leading}}^{\mathrm{sub}}} \quad t = 1,...,T \tag{34}$$

$$-\frac{P_{i,t}^{\mathrm{CG}}\sqrt{1-\left(\cos\varphi_{i,\min,\mathrm{lagging}}^{\mathrm{CG}}\right)^2}}{\cos\varphi_{i,\min,\mathrm{lagging}}^{\mathrm{CG}}}\le Q_{i,t}^{\mathrm{CG}}\le\frac{P_{i,t}^{\mathrm{CG}}\sqrt{1-\left(\cos\varphi_{i,\min,\mathrm{leading}}^{\mathrm{CG}}\right)^2}}{\cos\varphi_{i,\min,\mathrm{leading}}^{\mathrm{CG}}}$$
$$\forall i\in\Omega_{\mathrm{CG}};t=1,...,T \tag{35}$$

$$-\frac{P_{i,t}^{\mathrm{PV}}\sqrt{1-\left(\cos\varphi_{i,\min,\mathrm{lagging}}^{\mathrm{PV}}\right)^2}}{\cos\varphi_{i,\min,\mathrm{lagging}}^{\mathrm{PV}}}\le Q_{i,t}^{\mathrm{PV}}\le\frac{P_{i,t}^{\mathrm{PV}}\sqrt{1-\left(\cos\varphi_{i,\min,\mathrm{leading}}^{\mathrm{PV}}\right)^2}}{\cos\varphi_{i,\min,\mathrm{leading}}^{\mathrm{CG}}}$$
$$\forall i\in\Omega_{\mathrm{PV}};t=1,...,T \tag{36}$$

$$-\frac{P_{i,t}^{\mathrm{W}}\sqrt{1-\left(\cos\varphi_{i,\min,\mathrm{lagging}}^{\mathrm{W}}\right)^2}}{\cos\varphi_{i,\min,\mathrm{lagging}}^{\mathrm{W}}}\le Q_{i,t}^{\mathrm{W}}\le\frac{P_{i,t}^{\mathrm{W}}\sqrt{1-\left(\cos\varphi_{i,\min,\mathrm{leading}}^{\mathrm{W}}\right)^2}}{\cos\varphi_{i,\min,\mathrm{leading}}^{\mathrm{CG}}}$$
$$\forall i\in\Omega_{\mathrm{W}};t=1,...,T \tag{37}$$

where:

$\cos\varphi_{\min,\mathrm{leading}}^{\mathrm{MG}},\cos\varphi_{i,\min,\mathrm{leading}}^{\mathrm{CG}},\cos\varphi_{i,\min,\mathrm{leading}}^{\mathrm{PV}},\cos\varphi_{i,\min,\mathrm{leading}}^{\mathrm{W}}$ are the minimum leading power factors at node *i*;

$\cos\varphi_{\min,\mathrm{lagging}}^{\mathrm{MG}},\cos\varphi_{i,\min,\mathrm{lagging}}^{\mathrm{CG}},\cos\varphi_{i,\min,\mathrm{lagging}}^{\mathrm{PV}},\cos\varphi_{i,\min,\mathrm{lagging}}^{\mathrm{W}}$ are the minimum lagging power factors at node *i*.

2.2.2. *Linearization of Power Flow Constraints*

Set $I_{i,t}^{\mathrm{sqr}}=I_{i,t}^2$ and $U_{i,t}^{\mathrm{sqr}}=U_{i,t}^2$, the equations (38) – (43) can be illustrated as follows:

$$\sum_{k\in\Omega_{pr(i)}}\left(P_{ki,t}-r_{ki}I_{ki,t}^{\mathrm{sqr}}\right)-\sum_{j\in\Omega_{cr(i)}}P_{ij,t}=P_{i,t}^{\mathrm{D}}-P_{i,t}^{\mathrm{sub,B}}$$
$$+P_{i,t}^{\mathrm{Ch}}+P_{i,t}^{\mathrm{sub,S}}-P_{i,t}^{\mathrm{Dch}}-P_{i,t}^{\mathrm{CG}}-P_{i,t}^{\mathrm{PV}}-P_{i,t}^{\mathrm{W}} \tag{38}$$
$$\forall j\in\Omega_{cr(i)};i\in\Omega_{\mathrm{B}};t=1,...,T$$

$$U_{i,t}^{\mathrm{sqr}}-U_{j,t}^{\mathrm{sqr}}-2\left(r_{ij}P_{ij,t}+x_{ij,t}Q_{ij,t}\right)+\left(r_{ij}^2+x_{ij}^2\right)I_{ij,t}^{\mathrm{sqr}}=0 \tag{39}$$
$$\forall j\in\Omega_{cr(i)};i\in\Omega_{\mathrm{B}};t=1,...,T \tag{40}$$

$$I_{ij,t}^{\mathrm{sqr}}U_{i,t}^{\mathrm{sqr}}=P_{ij,t}^2+Q_{ij,t}^2;\ \forall i\in\Omega_{\mathrm{B}};t=1,...,T \tag{41}$$

$$\left(I_{ij}^{\min}\right)^2\le I_{ij,t}^{\mathrm{sqr}}\le\left(I_{ij}^{\max}\right)^2\ ;\ \forall j\in\Omega_{cr(i)};i\in\Omega_L;t=1,...,T \tag{42}$$

$$\left(U_{\min}\right)^2\le U_{i,t}^{\mathrm{sqr}}\le\left(U_{\max}\right)^2\ ;\ \forall i\in\Omega_{\mathrm{B}};t=1,...,T \tag{43}$$

Constraint (41) is a nonlinear equation, therefore, the authors will linearize this constraint using the piecewise linearization method [15]. Based on [16], the left-hand side of expression (41) is linearized by segmenting the variable $U_{i,t}^{\mathrm{sqr}}=U_{i,t}^2$ through the binary variable $\gamma_{i,s}$. The binary variable $\gamma_{i,s}$ is equal to 1 if and only if $U_{i,t}^{\mathrm{sqr}}$ has a value greater than $\left(U_{\min}^2+s\Delta U^{\mathrm{sqr}}\right)$. This is expressed in constraints (44)–(49).

$$I_{ij,t}^{\mathrm{sqr}}U_{i,t}^{\mathrm{sqr}}=\left(U_{\min}^2+\frac{1}{2}\Delta U\right)I_{ij,t}^{\mathrm{sqr}}+\sum_{s=1}^{S}P_{i,s}^{c}$$
$$\forall ij\in\Omega_{\mathrm{L}};t=1,...,T \tag{44}$$

$$\begin{cases}U_{i,t}^{\mathrm{sqr}}\ge U_{\min}^2+\sum_{s=1}^{S}\left(\gamma_{i,s}\Delta U\right)\\ U_{i,t}^{\mathrm{sqr}}\le U_{\min}^2+\Delta U+\sum_{s=1}^{S}\left(\gamma_{i,s}\Delta U\right)\end{cases}\quad\forall i\in\Omega_{\mathrm{B}} \tag{45}$$

$$\gamma_{i,s}\in\{0,1\}\ ;\ \forall i\in\Omega_{\mathrm{B}};s=1,....,S \tag{46}$$

$$\gamma_{i,s}\le\gamma_{i,s-1}\ ;\ \forall i\in\Omega_{\mathrm{B}};s=1,....,S \tag{47}$$

$$0\le I_{ij,t}^{\mathrm{sqr}}\Delta U-P_{i,s}^{c}\le\left(I_{ij}^{\max}\right)^2\Delta U\left(1-\gamma_{i,s}\right)$$
$$\forall ij\in\Omega_{\mathrm{L}};t=1,...,T;s=1,...,S \tag{48}$$

$$0\le P_{i,s}^{c}\le\left(I_{ij}^{\max}\right)^2\gamma_{i,s}\Delta U$$
$$\forall ij\in\Omega_{\mathrm{L}};t=1,...,T;s=1,...,S \tag{49}$$

where:

- ΔU is the length of the linear segment of the variable $U_{i,t}^{\mathrm{sqr}}$ (pu) and is defined as:

$$\Delta U=\frac{U_{\max}^2-U_{\min}^2}{S+1} \tag{50}$$

with *S* being the number of linear segments of the variable $U_{i,t}^{\mathrm{sqr}}$;

- $P_{i,s}^{c}$ is the correction power used in the piecewise linearization of $U_{i,t}^{\mathrm{sqr}}I_{ij,t}^{\mathrm{sqr}}$ (pu);
- $\gamma_{i,s}$ is the binary variable used in the piecewise linearization of $U_{i,t}^{\mathrm{sqr}}$;

Constraint (44) describes the linear approximation of the product of two continuous variables $U_{i,t}^{\mathrm{sqr}}$ and I_{ij}^{sqr}. Specifically, the product of these two variables is calculated by taking half the length of the first segment of the variable $U_{i,t}^{\mathrm{sqr}}$ and multiplying it by I_{ij}^{sqr}, and then adding the correction power $P_{i,s}^{\mathrm{c}}$. Constraints (48) and (49) show how to determine the correction power $P_{i,s}^{\mathrm{c}}$ depending on the length of the linear segment ΔU. If $\gamma_{i,s}=0$ then $P_{i,s}^{c}=0$ and . Conversely, $I_{ij,t}^{\mathrm{sqr}}\le\left(I_{ij}^{\max}\right)^2$ when $\gamma_{i,s}=1$, then $I_{ij}^{\mathrm{sqr}}\Delta U=P_{i,s}^{c}$ and $P_{i,s}^{c}\le\left(I_{ij}^{\max}\right)^2\Delta U$. Thus, $\left(I_{ij}^{\max}\right)^2\Delta U$ serves to make the boundary of $P_{i,s}^{\mathrm{c}}$ large enough.

Following this, the right-hand side of expression (41) is linearized as follows:

$$P_{ij,t}^2+Q_{ij,t}^2=\sum_{r=1}^{R}\delta_{ij,t,r}\left(\Delta P_{ij,t,r}+\Delta Q_{ij,t,r}\right)$$
$$\forall ij\in\Omega_{\mathrm{L}};t=1,...,T \tag{51}$$

$$P_{ij,t}^{+}-P_{ij,t}^{-}=P_{ij,t}\ ;\ \forall ij\in\Omega_{\mathrm{L}};t=1,...,T \tag{52}$$

$$Q_{ij,t}^{+}-Q_{ij,t}^{-}=Q_{ij,t}\ ;\ \forall ij\in\Omega_{\mathrm{L}};t=1,...,T \tag{53}$$

$$P_{ij,t}^{+}+P_{ij,t}^{-}=\sum_{r=1}^{R}\Delta P_{ij,t,r}\ ;\ \forall ij\in\Omega_{\mathrm{L}};t=1,...,T \tag{54}$$

$$Q_{ij,t}^{+}+Q_{ij,t}^{-}=\sum_{r=1}^{R}\Delta Q_{ij,t,r}\ ;\ \forall ij\in\Omega_{\mathrm{L}};t=1,...,T \tag{55}$$

$$0\le P_{ij,t,r}\le\Delta S_{ij}\ ;\ \forall ij\in\Omega_{\mathrm{L}};t=1,...,T;r=1,...,R \tag{56}$$

$$0\le Q_{ij,t,r}\le\Delta S_{ij}\ ;\ \forall ij\in\Omega_{\mathrm{L}};t=1,...,T;r=1,...,R \tag{57}$$

$$0\le P_{ij,t}^{+},P_{ij,t}^{-},Q_{ij,t}^{+},Q_{ij,t}^{-}\ ;\ \forall ij\in\Omega_{\mathrm{L}};t=1,...,T \tag{58}$$

$$\Delta S_{ij} = \frac{S_{\max}}{R};\ \forall ij \in \Omega_L; t = 1,...,T \quad (59)$$

$$\delta_{ij,t,s} = (2r-1)\Delta S_{ij}$$
$$\forall ij \in \Omega_L; t = 1,...,T; r = 1,...,R \quad (60)$$

where:

- $\Delta P_{ij,t,r}$ và $\Delta Q_{ij,t,r}$ are the r-th linear segment values of $|P_{ij,t}|$ and $|Q_{ij,t}|$ (pu);
- $P^{+}_{ij,t}, P^{-}_{ij,t}$ are non-negative auxiliary variables used to determine $|P_{ij,t}|$ (pu);
- $Q^{+}_{ij,t}, Q^{-}_{ij,t}$ are non-negative auxiliary variables used to determine $|Q_{ij,t}|$ (pu);
- ΔS_{ij} is a constant representing the upper limit of each linear segment of $|P_{ij,t}|$ and $|Q_{ij,t}|$ (pu);
- $\delta_{ij,t,r}$ is a constant representing the slope of the r-th linear segment of $|P_{ij,t}|$ and $|Q_{ij,t}|$ (pu);
- r is the number of linear segments of $|P_{ij,t}|$ and $|Q_{ij,t}|$.

Expression (51) is the right-hand side of constraint (41) after it has been transformed by linearization. Constraints (52)–(55) represent the relationship between the non-negative auxiliary variables and $P_{ij,t}$, $Q_{ij,t}$. The limits of the linear segments and auxiliary variables are presented in constraints (56)–(58). Equations (59) and (60) respectively show how to determine the constant values ΔS_{ij} and $\delta_{ij,t,r}$.

Combining equations (44) and (51), constraint (41) can be rewritten as follows:

$$\begin{bmatrix} \left(U^2_{\min} + \frac{1}{2}\Delta V\right) I^{\text{sqr}}_{ij,t} \\ + \sum_{s=1}^{S} P^{c}_{i,s} \end{bmatrix} = \sum_{r=1}^{R} \delta_{ij,t,r} \begin{pmatrix} \Delta P_{ij,t,r} \\ + \Delta Q_{ij,t,r} \end{pmatrix} \quad (61)$$

$$\forall ij \in \Omega_L; t = 1,...T$$

The MIQP model for the day-ahead scheduling problem, considering grid constraints, has an objective function represented by equation (1). The constraints include:

- Constraints on the power exchange between the microgrid and the main grid: (2)–(4) and (34);
- Constraints on conventional power sources, including: (6)–(7), (9)–(16), and (35);
- Constraints on renewable energy sources: (17), (18), (36), and (37);
- Constraints on energy storage devices: (21)–(33);
- Linearized power flow constraints for the grid, including (38)–(40), (42)–(43), and (61);
- Piecewise linearized constraints for equation (41), as presented in (45)–(49) and (52)–(60).

3. Results and Discussion

In this section, the IEEE 33-bus small power grid [7] is used for calculation with the proposed optimization model discussed in Section 2. The proposed optimization method is programmed using the GAMS language along with the commercial solver CPLEX [17]. A personal computer with a Core i5-10300H 2.50 GHz processor and 8GB RAM was used to perform the calculations.

3.1. IEEE 33-Bus Small Power Grid Data

The IEEE 33-bus power grid has a diagram as shown in Figure 1. The nominal voltage and base power are 12.66 kV and 100 kVA, respectively. The required voltage limits are $0.95 \le U \le 1.05$ pu. All branches have the same power transfer limit of 5 MVA.

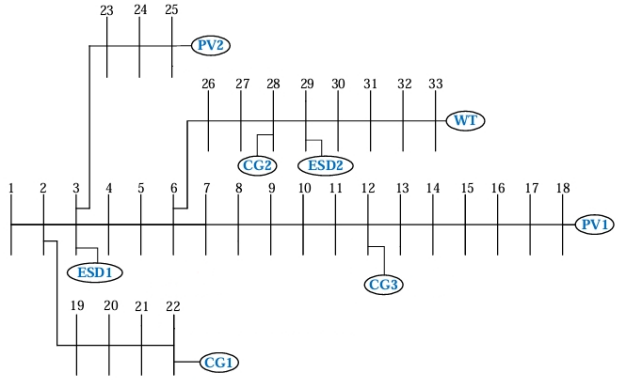

Figure 1: Modified IEEE 33-Bus Power Grid

The technical specifications for the two energy storage devices, ESD1 and ESD2, are identical. Specifically, each storage device has a capacity of 1000 kWh; a maximum charging/discharging power of 500 kW; a minimum energy level of 200 kWh; a maximum energy level of 900 kWh; a charging/discharging efficiency of 90%, and an initial energy level of 200 kWh.

The small power grid operates in grid-connected mode during the following hours: 5, 6, 11, 15, 16, 17, 22, and 23. At other times, it operates in islanded mode. During grid-connected mode, electricity purchase or sale between the small power grid and the main grid is allowed, subject to a power exchange limit of 1000 kW. The day-ahead electricity price at the MG connection point is shown in Figure 2.

The forecast data for the renewable energy sources and load power at each time step are referenced from [18] and presented as a percentage of their maximum power, as shown in Figure 3. Specifically, the maximum load power is 3715 + j2300 kVA. Both wind and solar power sources have a maximum power of 1000 kW. The power flow equations are linearized with 20 segments

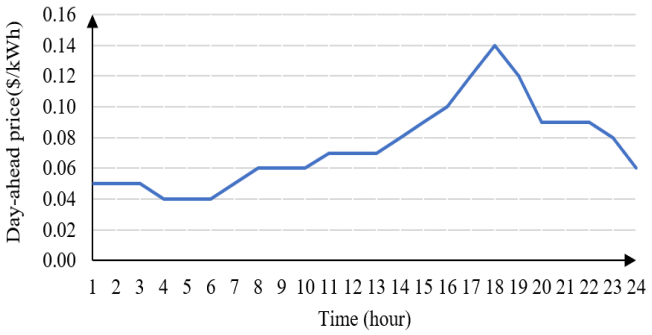

Figure 2: Next-Day Electricity Price at the MG Connection Point.

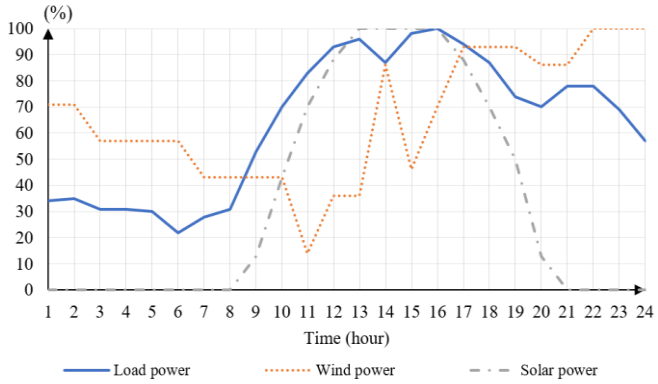

Figure 3: Graph of percentage relative to maximum power for load, wind, and solar power over time.

3.2. Calculation Results

In this section, the paper presents the results of the proposed model's calculation. The small power grid is operated in grid-connected/islanded mode at the specific times described in Section 3.1.

Table 1: Next-Day Operational Schedule for Traditional Power Sources

t (h)	CG1	CG2	CG3
1	1	1	0
2	1	1	0
3	1	1	0
4	1	1	0
5	1	0	0
6	1	0	0
7	1	0	0
8	1	1	0
9	1	1	0
10	1	1	1
11	1	1	1
12	1	1	1
13	1	1	1
14	1	1	0
15	1	1	0
16	1	1	0
17	1	1	0
18	1	1	0
19	1	1	0
20	1	1	1
21	1	1	1
22	1	1	1
23	1	0	1
24	1	0	1

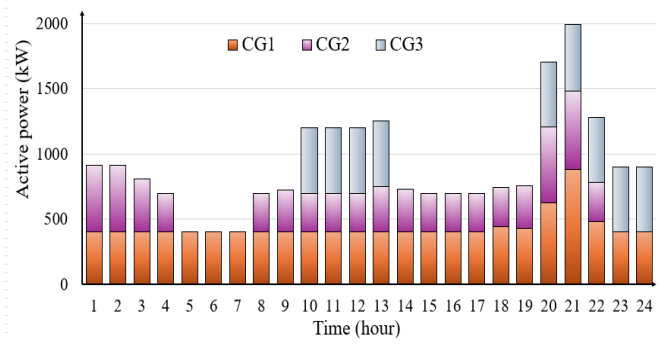

Figure 4: Active Power from Traditional Power Plants.

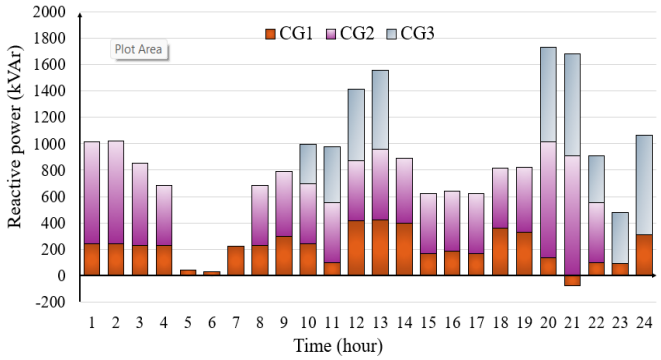

Figure 5: Reactive Power from Traditional Power Plants.

The results of the next-day operation scheduling for the 3 traditional power plants, as shown in Table 1, indicate that unit CG1 operates continuously throughout the scheduling cycle, while units CG2 and CG3 alternate between operation and rest periods.

The calculated power generation of the traditional power plants during grid-connected and islanded modes of the MG is presented in Figures 4 and 5. It is observed that CG1 operates in base-load mode, and CG3 operates in peak-load mode.

Renewable energy sources are clean and have negligible operational costs. Consequently, the wind and solar power sources operate continuously for 24 hours, generating power equal to the forecasted value shown in Figure 3.

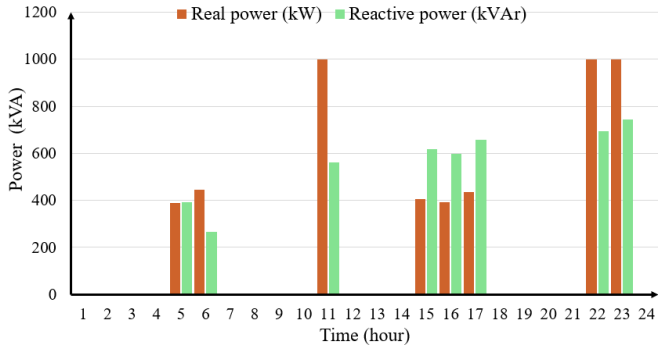

Figure 6: Power Exchange between the Small Power Grid and the Main Grid

The power exchange between the MG and the main grid is illustrated in Figure 6. The small power grid consistently purchases electricity from the main grid during grid-connected periods. Notably, it purchases electricity at the maximum allowable power of 1000 kW during hours t = 11, t = 22, and t = 23. At t = 5 and t = 6, the power purchases are 388 kW and 446 kW, respectively. Additionally, the distribution grid sells 407 kW, 393 kW, and 434 kW to the MG at hours t = 15, t = 16, and t = 17.

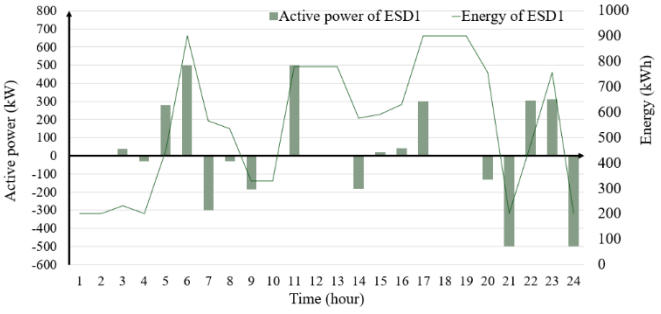

Figure 7: Charging/Discharging Power and Energy Level of ESD1 in the Small Power Grid

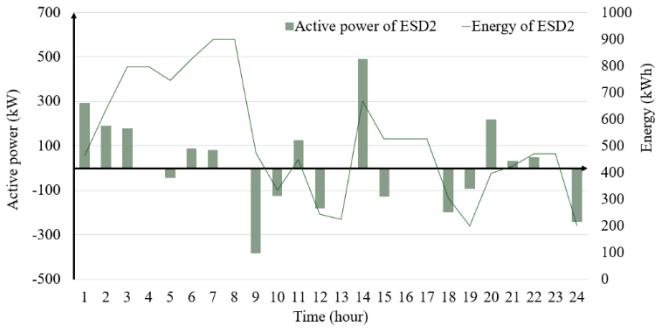

Figure 8: Charging/Discharging Power and Energy Level of ESD2 in the Small Power Grid.

Figures 7 and 8 illustrate the energy level and charging/discharging power of the two energy storage devices, ESD1 and ESD2, over a 24-hour period. Positive power values represent charging, while negative values correspond to discharging. It can be seen that during periods of low load power, the energy storage devices tend to charge, whereas during periods of high load power, the devices discharge. ESD1 reaches its maximum energy level at hours t = {6, 17, 18, 19}, storing a total of 13,165 kWh. Similarly, ESD2 achieves its maximum energy level at hours t = 7 and t = 8 with a total energy of 12,499 kWh.

Figure 9 presents the voltage distribution across the 33 buses at three different times. At t = 15, node voltages are generally lower than at t = 5 and t = 22. At t = 5, since the load power is low, the voltage at most nodes is higher compared to the other two times.

Additionally, Figure 10 shows the 24-hour voltage distribution at nodes 8, 12, and 29. Node 12 has the traditional power source CG1, while node 29 is connected to the energy storage device ESD2.

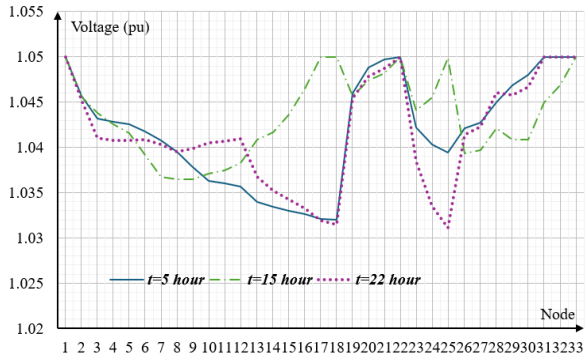

Figure 9: Voltage Distribution at t = 5, t = 15, and t = 22.

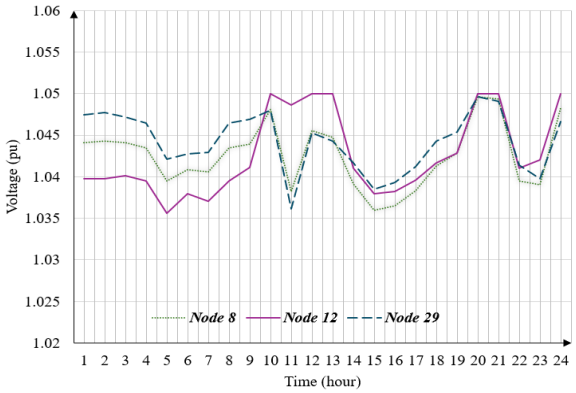

Figure 10: 24-Hour Voltage Distribution at Nodes 8, 12, and 29 of the MG

3.3. Impact of the Small Power Grid's Operation Mode

To examine the impact of the operation mode of the small power grid, this paper compares the operational schedules of the traditional power sources, the energy levels, the charging/discharging power of ESD1, and the power exchange between the small power grid and the main grid under two scenarios:

− **Scenario 1 (SC1)**: The MG operates in both grid-connected and islanded mode.

− **Scenario 2 (SC2)**: The MG operates exclusively in grid-connected mode for 24 hours.

The operation states of the traditional power sources under both scenarios are presented in Table 2 (with values in parentheses indicating changes when the MG operates exclusively in grid-connected mode for 24 hours). From Table 2, it is evident that the operation mode of the MG significantly influences the operational states of the generating units.

Table 2: Optimal Operational States of Traditional Power Sources in Scenario 1/Scenario 2.

t (h)	CG1	CG2	CG3
1	1	1	0
2	**1 (0)**	1	0
3	**1 (0)**	1	0
4	**1 (0)**	1	0
5	**1 (0)**	**0 (1)**	0
6	**1 (0)**	**0 (1)**	0
7	**1 (0)**	**0 (1)**	0
8	**1 (0)**	1	0
9	1	1	0
10	1	1	**1 (0)**
11	1	1	**1 (0)**
12	1	1	**1 (0)**
13	1	1	**1 (0)**
14	1	1	0
15	1	1	0
16	1	1	0
17	1	1	0
18	1	**1 (0)**	0
19	1	**1 (0)**	0
20	1	**1 (0)**	1
21	1	**1 (0)**	1
22	1	**1 (0)**	1
23	1	0	1

Figure 11 shows a comparison of the power generation of CG1 in both scenarios. In Scenario 1, CG1 operates continuously for 24 hours with varying power output. In Scenario 2, CG1 ceases operation from t = 2 to t = 8 and operates at minimum power during the remaining periods. From Table 3, it is evident that when operating in grid-connected mode for 24 hours (Scenario 2), the MG sells power to the main grid at t = 18. At all other times, the MG purchases power from the main grid. In Scenario 2, the amount of electricity purchased by the MG from the main grid over 24 hours is 11,757 kWh. In contrast, under Scenario 1, the total electricity purchased by the MG from the main grid over 24 hours is 5,068 kWh.

The operating status of ESD1 in the two scenarios is presented in Table 4. From Table 4, we can see that the MG's operating mode significantly impacts the operation of ESD1. The total energy consumption of ESD1 over one day under Scenario 2 is

14,483 kWh. This value is higher than the total energy consumption for ESD1 in one day under Scenario 1 (13,165 kWh).

Additionally, the total operational cost in Scenario 1 and Scenario 2 is $9,563.40 and $6,481.50, respectively. Thus, it can be seen that the operational cost in Scenario 2 has decreased by 32.2% compared to Scenario 1. The reason is that the operating states of the traditional units (CG1, CG2, and CG3) in the two scenarios are different. This difference leads to changes in the electricity purchased from the external grid, the charging and discharging power of the energy storage system, and the generation power of traditional power sources.

Table 3: Comparison of Power Exchange between the Small Power Grid and the Main Grid in Both Scenarios.

t (h)	Active Power (kW)		Reactive Power (kVAr)	
	SC 1	SC 2	SC 1	SC 2
1	0	861	0	279
2	0	321	0	488
3	0	281	0	426
4	0	281	0	426
5	388	288	392	437
6	446	343	267	260
7	0	298	0	312
8	0	276	0	318
9	0	716	0	224
10	0	589	0	280
11	1000	501	560	604
12	0	434	0	621
13	0	422	0	641
14	0	496	0	722
15	407	407	618	618
16	393	393	597	596
17	434	419	659	635
18	0	-17	0	0
19	0	74	0	112
20	0	1000	0	460
21	0	1000	0	697
22	1000	1000	693	741
23	1000	1000	744	710
24	0	358	0	544

Table 4. Comparison of charging/discharging power and energy levels of ESD1 in the two scenarios.

t (h)	Charging Power (kW)		Discharging Power (kW)		Energy Level (kWh)	
	SC 1	SC 2	SC1	SC2	SC1	SC2
1	0	500	0	0	200	650
2	0	0	0	50	200	594
3	36	0	0	12	233	581
4	0	0	30	12	200	567
5	278	33	0	0	450	597
6	500	106	0	0	900	692
7	0	0	300	18	567	672
8	0	0	29	152	535	503
9	0	127	185	0	329	617
10	0	0	0	0	329	617
11	500	0	0	0	779	617
12	0	0	0	78	779	530
13	0	0	0	28	779	499
14	0	428	183	0	576	884
15	18	0	0	0	593	884
16	42	0	0	0	630	884
17	299	17	0	0	900	900
18	0	0	0	434	900	418
19	0	0	0	196	900	200
20	0	397	130	0	756	557
21	0	0	500	11	200	545
22	305	0	0	23	475	519
23	312	262	0	0	756	756
24	0	0	500	500	200	200

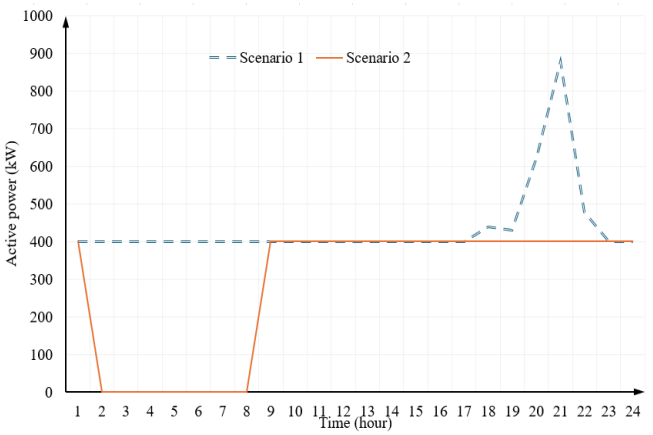

Figure 11. Generation power of CG1 in Scenario 1 and Scenario 2.

3.4. Effectiveness evaluation of the proposed optimization model

The computational efficiency of the proposed optimization model is compared with intelligent computational methods (metaheuristic algorithms) using small power grids in rural Africa [19]. It is emphasized that the intelligent computing methods in [19] only apply to the UC problem without considering constraints on the ramp-up and ramp-down rates of generation, minimum up/down times of traditional power sources, and the power network. Comparison of the optimal operating cost (objective function value) of the proposed optimization method with the metaheuristic methods [19] using small-scale grids in rural Africa is presented in Table 5.

Table 5. Comparison of the objective function values.

Method	Value of objective function ($)
GWO	3122
MGWO	3120
MGWOSCA	3119
MGWOCSA	3118
MGWOPSO	3116
Proposed MIQP model	3111.2

Table 5 shows that the objective function value calculated using the proposed method is lower (0.17÷0.36)% compared to the metaheuristic methods.

4. Conclusion

This study proposes a MIQP model to plan the next-day operation of an MG, incorporating grid-connected/islanded operation modes and grid constraints. The objective function of the model is to minimize the operational costs of the MG. The proposed model was applied to the 33-bus IEEE microgrid to assess its effectiveness. The computational results indicate that the MG purchases electricity from the main grid during most periods in both operational scenarios (grid-connected/islanded and 24-hour grid-connected scenarios). Furthermore, when the MG remains connected to the grid for 24 hours, all traditional power sources operate at their minimum output levels. This demonstrates that the MG prioritizes purchasing electricity from the main grid due to its lower cost. Consequently, the operating mode of the MG significantly affects the optimal operation planning of the microgrid. The research results also show that energy storage devices tend to charge

during periods of low load power and discharge during periods of high load power. Future research will focus on developing an optimal MILP model for day-ahead operation planning of MGs under uncertainty.

APPENDIX

Table A1: Parameters of Traditional Power Sources

Parameter	CG1	CG2	CG3
Variable cost ($/kW²h)	0.00015	0.00025	0.00035
Variable cost ($/kWh)	0.2881	0.3476	0.2571
Fixed cost ($/h)	7.5	0	20
Start-up cost ($)	15	10	7.5
Shutdown cost ($)	5.3	0	1.5
Maximum output (kW)	1000	800	1500
Minimum output (kW)	400	300	500
Power increase/decrease limit (kW/h)	400	300	500
Power increase/decrease limit at start-up/shutdown (kW/h)	400	300	500
Minimum operating time (h)	2	3	4
Minimum rest time (h)	2	3	4
Initial state	ON	ON	OFF
Initial output	500	100	-
Hours worked before cycle (h)	2	3	-
Hours rested before cycle (h)	-	-	4

Table A2: Maximum Load Power of the Microgrid

Node	P (kW)	Q (kVAr)	Node	P (kW)	Q (kVAr)
2	100	60	**18**	90	40
3	90	40	**19**	90	40
4	120	80	**20**	90	40
5	60	30	**21**	90	40
6	60	20	**22**	90	40
7	200	100	**23**	90	50
8	200	100	**24**	420	200
9	60	20	**25**	420	200
10	60	20	**26**	60	25
11	45	30	**27**	60	25
12	60	35	**28**	60	20
13	60	35	**29**	120	70
14	120	80	**30**	200	600
15	60	10	**31**	150	70
16	60	20	**32**	210	100
17	60	20	**33**	60	40

Table A3: Branch Data

No.	From node	To node	r (Ω)	x (Ω)	S_{max} (MVA)
1	**1**	**2**	0.0922	0.047	5
2	**2**	**3**	0.493	0.2511	5
3	**3**	**4**	0.366	0.1864	5
4	**4**	**5**	0.3811	0.1941	5
5	**5**	**6**	0.819	0.707	5
6	**6**	**7**	0.1872	0.6188	5
7	**7**	**8**	0.7114	0.2351	5
8	**8**	**9**	1.03	0.74	5
9	**9**	**10**	1.044	0.74	5
10	**10**	**11**	0.1966	0.066	5
11	**11**	**12**	0.3744	0.1238	5
12	**12**	**13**	1.468	1.155	5
13	**13**	**14**	0.5416	0.7129	5
14	**14**	**15**	0.591	0.526	5
15	**15**	**16**	0.7463	0.545	5
16	**16**	**17**	1.289	1.721	5
17	**17**	**18**	0.732	0.574	5
18	**2**	**19**	0.164	0.1565	5
19	**19**	**20**	1.5042	1.3554	5
20	**20**	**21**	0.4095	0.4784	5
21	**21**	**22**	0.7089	0.9373	5
22	**3**	**23**	0.4512	0.3083	5
23	**23**	**24**	0.898	0.7091	5
24	**24**	**25**	0.896	0.7011	5
25	**6**	**26**	0.203	0.1034	5
26	**26**	**27**	0.2842	0.1447	5
27	**27**	**28**	1.059	0.9337	5
28	**28**	**29**	0.8042	0.7006	5
29	**29**	**30**	0.5075	0.2585	5
30	**30**	**31**	0.9744	0.963	5
31	**31**	**32**	0.3105	0.3619	5
32	**32**	**33**	0.341	0.5302	5

References

[1] N. Hatziargyriou, H. Asano, R. Iravani, and C. Marnay, "Microgrids," *IEEE Power and Energy Mag.*, vol. 5, no. 4, pp. 78–94, Jul. 2007, https:10.1109/MPAE.2007.376583.

[2] N. V. Pham, T. H. T. Nguyen, V. H. Trinh, and Q. C. Vu, "A MILP-based formulation for thermal-wind-bess unit commitment problem considering network power loss," *TNUJST*, vol. 227, no. 16, pp. 85–93, Oct. 2022, doi: 10.34238/tnu-jst.6485.

[3] P. N. V. Pham, "Power flow incorporating cost-based droop control strategies for ac autonomous microgrids," *JST-UD*, pp. 28–32, Dec. 2020, doi: 10.31130/jst-ud2020-124E.

[4] X. Li, W. Wang, H. Wang, J. Wu, X. Fan, and Q. Xu, "Dynamic environmental economic dispatch of hybrid renewable energy systems based on tradable green certificates," *Energy*, vol. 193, p. 116699, Feb. 2020, doi: 10.1016/j.energy.2019.116699.

[5] Y. Bai, X. Wu, and A. Xia, "An enhanced multi-objective differential evolution algorithm for dynamic environmental economic dispatch of power system with wind power," *Energy Science & Engineering*, vol. 9, no. 3, pp. 316–329, Mar. 2021, doi: 10.1002/ese3.827.

[6] A. K. Basu, S. Chowdhury, and S. P. Chowdhury, "Impact of Strategic Deployment of CHP-Based DERs on Microgrid Reliability," *IEEE Trans. Power Delivery*, vol. 25, no. 3, pp. 1697–1705, Jul. 2010, doi: 10.1109/TPWRD.2010.2047121.

[7] N. Zaree and V. Vahidinasab, "An MILP formulation for centralized energy management strategy of microgrids," in *2016 Smart Grids Conference (SGC)*, Kerman, Iran: IEEE, Dec. 2016, pp. 1–8. doi: 10.1109/SGC.2016.7883464.

[8] M. Farrokhabadi, C. A. Canizares, and K. Bhattacharya, "Unit Commitment for Isolated Microgrids Considering Frequency Control," *IEEE Trans. Smart Grid*, vol. 9, no. 4, pp. 3270–3280, Jul. 2018, doi: 10.1109/TSG.2016.2629982.

[9] Y. Zhang, Q. Wu, H. Ren, Q. Li, and W. Zhou, "Optimal operation of multi-microgrid systems considering multi-level energy-certificate-carbon coupling trading," *Renewable Energy*, vol. 227, p. 120505, Jun. 2024, doi: 10.1016/j.renene.2024.120505.

[10] T. H. B. Huy, T.-D. Le, P. V. Phu, S. Park, and D. Kim, "Real-time power scheduling for an isolated microgrid with renewable energy and energy storage system via a supervised-learning-based strategy," *Journal of Energy Storage*, vol. 88, p. 111506, May 2024, doi: 10.1016/j.est.2024.111506.

[11] X. Han, Z. Li, Z. Li, Y. Zhao, and M. Ban, "Privacy-Preserving Operational Decision Making for Networked Autonomous Microgrids Based on Bilevel Mixed-Integer Optimization," *IEEE Trans. Smart*

Grid, vol. 15, no. 3, pp. 2881–2897, May 2024, doi: 10.1109/TSG.2023.3323789.

[12] S. Shakerinia, A. F. Meyabadi, M. Vahedi, N. Salehi, and M. S. Moghaddam, "Optimal Operation of Microgrids With Worst-Case Renewable Energy Outage: A Mixed-Integer Bi-Level Model," *IEEE Access*, vol. 11, pp. 59804–59815, 2023, doi: 10.1109/ACCESS.2023.3285480.

[13] X. Kong, D. Liu, C. Wang, F. Sun, and S. Li, "Optimal operation strategy for interconnected microgrids in market environment considering uncertainty," *Applied Energy*, vol. 275, p. 115336, Oct. 2020, doi: 10.1016/j.apenergy.2020.115336.

[14] A. K. Basu, A. Bhattacharya, S. Chowdhury, and S. P. Chowdhury, "Planned Scheduling for Economic Power Sharing in a CHP-Based Micro-Grid," *IEEE Trans. Power Syst.*, vol. 27, no. 1, pp. 30–38, Feb. 2012, doi: 10.1109/TPWRS.2011.2162754.

[15] A. L. Motto, F. D. Galiana, A. J. Conejo, and J. M. Arroyo, "Network-constrained multiperiod auction for a pool-based electricity market," *IEEE Trans. Power Syst.*, vol. 17, no. 3, pp. 646–653, Aug. 2002, doi: 10.1109/TPWRS.2002.800909.

[16] A. C. Rueda-Medina, J. F. Franco, M. J. Rider, A. Padilha-Feltrin, and R. Romero, "A mixed-integer linear programming approach for optimal type, size and allocation of distributed generation in radial distribution systems," *Electric Power Systems Research*, vol. 97, pp. 133–143, Apr. 2013, doi: 10.1016/j.epsr.2012.12.009.

[17] GAMS Development Corp, "GAMS Documentation 46," Feb. 2024. [Online]. Available: https://www.gams.com

[18] C. Deckmyn, J. Van De Vyver, T. L. Vandoorn, B. Meersman, J. Desmet, and L. Vandevelde, "Day-ahead unit commitment model for microgrids," *IET Generation, Transmission & Distribution*, vol. 11, no. 1, pp. 1–9, Jan. 2017, doi: 10.1049/iet-gtd.2016.0222.

[19] B. Dey and B. Bhattacharyya, "Hybrid Intelligence Techniques for Unit Commitment of Microgrids," in *2019 20th International Conference on Intelligent System Application to Power Systems (ISAP)*, New Delhi, India: IEEE, Dec. 2019, pp. 1–6. doi: 10.1109/ISAP48318.2019.9065950.